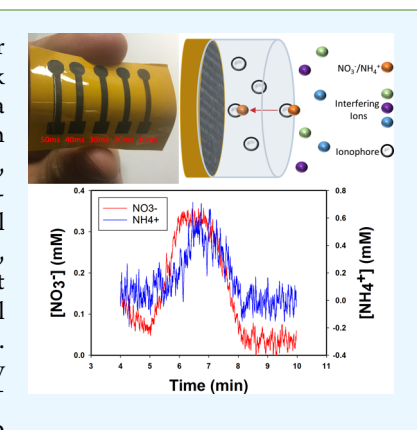
# Flexible Laser-Induced Graphene for Nitrogen Sensing in Soil

Nate T. Garland, Eric S. McLamore, Nicholas D. Cavallaro, Deyny Mendivelso-Perez, Emily A. Smith, ‡, Lo Dapeng Jing, and Jonathan C. Claussen\*, †, Lo

Supporting Information

ABSTRACT: Flexible graphene electronics are rapidly gaining interest, but their widespread implementation has been impeded by challenges with ink preparation, ink printing, and postprint annealing processes. Laser-induced graphene (LIG) promises a facile alternative by creating flexible graphene electronics on polyimide substrates through the one-step laser writing fabrication method. Herein, we demonstrate the use of LIG, created with a low-cost UV laser, for electrochemical ion-selective sensing of plantavailable nitrogen (i.e., both ammonium and nitrate ions: NH<sub>4</sub><sup>+</sup> and NO<sub>3</sub><sup>-</sup>) in soil samples. The laser used to create the LIG was operated at distinct pulse widths (10, 20, 30, 40, and 50 ms) to maximize the LIG electrochemical reactivity. Results illustrated that a laser pulse width of 20 ms led to a high percentage of sp<sup>2</sup> carbon (77%) and optimal peak oxidation current of 120 µA during cyclic voltammetry of ferro/ferricyanide. Therefore, LIG electrodes created with a 20 ms pulse width were consequently functionalized with distinct ionophores specific to NH<sub>4</sub><sup>+</sup> (nonactin) or NO<sub>3</sub><sup>-</sup> (tridodecylmethylammonium nitrate) within poly(vinyl chloride)-based membranes to



create distinct solid contact ion-selective electrodes (SC-ISEs) for NH<sub>4</sub><sup>+</sup> and NO<sub>3</sub><sup>-</sup> ion sensing, respectively. The LIG SC-ISEs displayed near Nernstian sensitivities of  $51.7 \pm 7.8 \text{ mV/dec } (\text{NH}_4^+) \text{ and } -54.8 \pm 2.5 \text{ mV/dec } (\text{NO}_3^-), \text{ detection limits of } 28.2 \text{ mV/dec } (\text{NO}_3^-) = 1.0 \text$  $\pm$  25.0  $\mu$ M (NH<sub>4</sub><sup>+</sup>) and 20.6  $\pm$  14.8  $\mu$ M (NO<sub>3</sub><sup>-</sup>), low long-term drift of 0.93 mV/h (NH<sub>4</sub><sup>+</sup> sensors) and -5.3  $\mu$ V/h (NO<sub>3</sub><sup>-</sup>) sensors), and linear sensing ranges of  $10^{-5}-10^{-1}$  M for both sensors. Moreover, soil slurry sensing was performed, and recovery percentages of 96% and 95% were obtained for added NH<sub>4</sub><sup>+</sup> and NO<sub>3</sub><sup>-</sup>, respectively. These results, combined with a facile fabrication that does not require metallic nanoparticle decoration, make these LIG electrochemical sensors appealing for a wide range of in-field or point-of-service applications for soil health management.

KEYWORDS: graphene, solid-contact ion-selective electrode (ISE), soil fertilizer, potentiometry, precision agriculture

### INTRODUCTION

Graphene-based electronics offer great promise for a wide variety of applications, including supercapacitors and batteries, graphene tattoo sensors, and other flexible electronics due to the unique material properties of graphene, such as high flexibility, electrical and thermal conductivity, and tensile strength.4 Challenges with realizing graphene-based electronics lie in relatively complex fabrication procedures, which have generally included chemical vapor deposition (CVD) and/or complex substrate-transfer techniques. CVD-synthesized carbon nanomaterials (carbon nanotubes or graphene) often require prepatterning a surface with metal catalysts (e.g., nickel, cobalt or iron) and carbon growth within a hightemperature (up to 1000 °C), low-pressure vacuum environment injected with carbon precursor gases. 5-8 However, alternative scalable manufacturing protocols for graphenebased electrical circuits are beginning to emerge, including solution-phase printing (inkjet printing, 9,10 screen printing, dispenser printing<sup>12</sup>) and direct laser scribing, <sup>13,14</sup> among

others. Solution phase printing techniques generally require an additional postprint processing step, such as thermal, 15 laser, 16 or photonic annealing 17,18 to improve electrical conductivity. High-temperature thermal annealing (250-400 °C<sup>10,19</sup>) of printed graphene is used to burn off nonconductive cellulosebased binders and solvents as well as to weld or sinter printed graphene flakes. However, thermal annealing is not conducive for use on thermally sensitive polymer or paper substrates. Others have used photonic annealing 18 or rapid-pulse laser annealing 15 that is conducive for thermally sensitive polymers, yet these methods require an additional postprint processing step that increases the electrode fabrication complexity. However, a recently discovered, promising alternative to printed graphene circuits is laser-induced graphene (LIG). 14,20,21

Received: July 2, 2018 Accepted: October 4, 2018 Published: October 4, 2018

<sup>†</sup>Mechanical Engineering Department, ‡Chemistry Department, and §Materials Analysis and Research Laboratory, Iowa State University, Ames, Iowa 50011, United States

Agricultural and Biological Engineering Department, Institute of Food and Agricultural Sciences, University of Florida, Gainesville, Florida 32611, United States

<sup>&</sup>lt;sup>1</sup>Ames Laboratory, Ames, Iowa 50011, United States

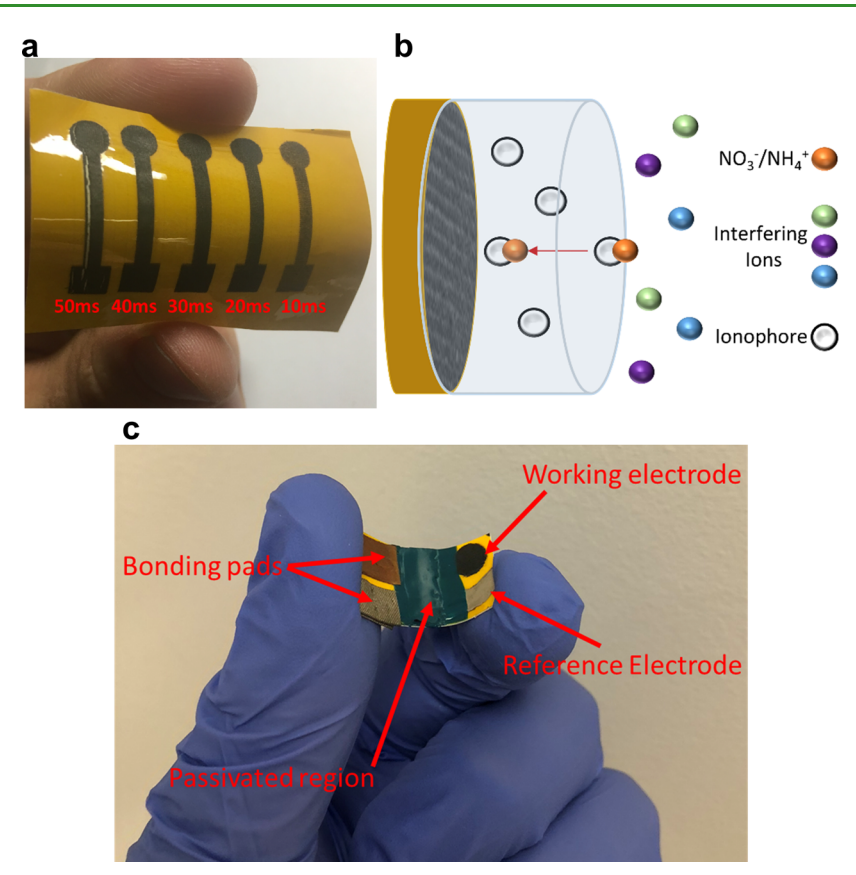


Figure 1. (a) Photograph of five LIG SC ISEs on a single polyimide swatch. (b) Illustration of SC-ISE ion sensing. (c) Representative electrode used in soil column studies. Passivated regions are shown as well as bonding pads, working electrode, and reference electrode.

LIG is a one-step lithography-free process upon which a laser converts sp<sup>3</sup>-hybridized carbon found in substrates, such as polyimide, into sp<sup>2</sup>-hybridized carbon: the carbon allotrope found in graphene. LIG is a versatile technique that has been used to produce graphene films that are superhydrophobic, doped with metal oxide nanocrystals,20 functionalized with polymer, 21 or developed into vertically aligned graphene fibers.<sup>23</sup> Typically, a rapid pulse (femtosecond), infrared (IR) laser is used to selectively transform distinct regions or patterns of polyimide film (Kapton tape) into sp<sup>2</sup>-hybridized carbon, viz., porous graphene. <sup>24–26</sup> This laser processing technique can be performed in air at room temperature without the need for prior patterning of the substrate with a metal catalyst or the need for chemical etching/cleaning techniques associated to CVD graphene fabrication. 5,27 This facile LIG manufacturing protocol also eliminates the need for ink preparation, ink printing, and postprint annealing processes associated with solution-phase printed graphene. 9,28,29 The utility of LIG has been displayed in numerous applications, including super-capacitors, <sup>14,22,30,31</sup> nonbiofouling surfaces, <sup>32</sup> transparent heaters,<sup>33</sup> and more recently, electrochemical sensors.<sup>25,26,34,35</sup> For example, a nonenzymatic amperometric glucose sensor comprised of LIG functionalized with Cu nanocubes was used to selectively measure glucose over a wide concentration range (25  $\mu$ M to 4 mM), which is physiologically relevant to glucose levels in saliva, tears, and blood.<sup>34</sup> In another report, a LIG electrode was used to monitor electroactive small molecules, including ascorbic acid, dopamine, and uric acid via cyclic voltammetry (CV) and differential pulse voltammetry.<sup>25</sup> Other recent biosensor examples include a LIG aptasensor developed for thrombin<sup>26</sup> and a LIG biosensor

for biogenic amines based on a nanocopper-diamine oxidase hybrid material.<sup>35</sup> However, ion sensing using LIG has yet to be demonstrated.

In this work, we demonstrate the first use of LIG for ion sensing by developing a solid-contact ion-selective electrode (SC-ISE). In addition, LIG is produced in this research by using a low-cost (\$100) consumer grade ultraviolet (UV) laser instead of a higher power, much more expensive  $CO_2$  IR laser used in previous studies. <sup>20,22–26,32,34</sup> UV lasers exhibit lower absorption and photothermal heating within the polyimide substrate and consequently, as shown herein, produce carbon structures that are a heterogeneous matrix of graphene and amorphous or graphitic carbon and less graphene-like than LIG produced with a CO<sub>2</sub> IR laser. However, given the intended use case of in-field, low-cost sensors, the UV laser was utilized in this study. CV, X-ray photoelectron spectroscopy (XPS), Raman spectroscopy, and scanning electron microscopy (SEM) characterization reveal that the laser scribing pulse widths (10, 20, 30, 40, and 50 ms) significantly alter the structure and electroactive nature of the LIG-based electrodes. The developed LIG electrodes are converted into SC-ISE by functionalization with a poly(vinyl chloride) (PVC) membrane containing an ionophore specific to NH<sub>4</sub><sup>+</sup> (nonactin) or NO<sub>3</sub><sup>-</sup> (tridodecylmethylammonium nitrate). The resulting nitrogen SC-ISE sensors display near Nernstian sensitivities of 51.7  $\pm$ 7.8 mV/dec  $(NH_4^{-+})$  and  $-54.8 \pm 2.5$  mV/dec  $(NO_3^{-})$ , detection limits of 28.2  $\pm$  25.0  $\mu$ M (NH<sub>4</sub><sup>+</sup>) and 20.6  $\pm$  14.8  $\mu M$  (NO<sub>3</sub><sup>-</sup>), linear sensing range of  $10^{-5}$ – $10^{-1}$  M, and relatively low long-term drifts (0.93 mV/h for NH<sub>4</sub><sup>+</sup> sensors and  $-5.3 \,\mu\text{V/h}$  for NO<sub>3</sub><sup>-</sup> sensors). The LIG ion sensors were used to measure NH<sub>4</sub><sup>+</sup> or NO<sub>3</sub><sup>-</sup> in a complex matrix (soil

slurry) with an average signal recovery of 96  $\pm$  14%. In soil column tests, transport of NH<sub>4</sub><sup>+</sup> and NO<sub>3</sub><sup>-</sup> followed expected trends, where higher soil column retention was observed for NH<sub>4</sub><sup>+</sup> and lower retention was observed for NO<sub>3</sub><sup>-</sup>. The recovery rate for LIG sensors was higher than 95% for all studies in complex soil matrices (nitrogen rich, and nitrogen poor soils), paving the way for future development of buryand-forget soil nitrogen sensors.

#### MATERIALS AND METHODS

LIG Electrode Fabrication. All chemicals used in the ISE membrane were obtained from Sigma-Aldrich. LIG electrodes were prepared with a standard high-temperature Kapton tape adhered to Epson printer paper (Kapton tape was placed on the emulsion side of the photopaper) followed by treatment with a 405 nm 1 W pulsed UV laser on two-dimensional (2D) stepper motors (HTPOW). The overall geometry (25.8 mm in length with a circular working area with diameter of 5.3 mm) of each electrode was first developed using computer-aided design. The laser pulse width governed the laser energy density per software provided with the equipment. The pulse width is defined by the manufacturer as the length of the laser pulse at each raster step. Laser pulse widths of 10, 20, 30, 40, and 50 ms were tested in an effort to maximize the electronic and electrochemical properties of the LIG electrodes. After laser graphitization of the polyimide, the LIG electrodes were passivated with an insulating lacquer, except for the 5.3 mm diameter region that acted as the working electrode (see Figure 1). Passivation prevented electrode short circuiting and nonspecific binding during electrochemical

LIG Functionalization for Ion-Selective Sensing. After graphitization of the polyimide, the LIG electrodes were functionalized with solid-contact ion-selective membranes (SC-ISM). The LIG electrodes were functionalized with either a NH<sub>4</sub><sup>+</sup>- or NO<sub>3</sub><sup>-</sup>selective SC-ISM. NH<sub>4</sub><sup>+</sup> ionophore cocktail was prepared by mixing nonactin, tetrakis-(4-chlorophenyl)-borate, dioctyl sebacate, and PVC (1/0.5/33.2/65.3 wt %, respectively) for a total mass of 100 mg. The NO<sub>3</sub><sup>-</sup> cocktail contained 0.25 (wt %) methyltriphenylphosphonium bromide, 1.93 (wt %) nitrocellulose dissolved in 35% 2-propanol, 16.25 (wt %) 2-nitrophenyl octyl ether, 5.75 (wt %) PVC, 74.32 (wt %) tetrahydrofuran (THF), and 1.5 (wt %) tridodecylmethylammonium nitrate. SC-ISM cocktails were dissolved in 1 mL THF followed by vortex mixing for ~1 min and overnight refrigeration to ensure homogeneity. To prepare SC-ISM on LIG, a 30  $\mu$ L aliquot of the ionselective cocktail was drop-cast onto the working electrode and allowed to dry overnight at room temperature in air. The resulting thickness of these ISMs was estimated by SEM imaging of crosssections of the resulting LIG-ISE (Figure S8 in Supporting Information). For n = 9 samples, the average thickness was 97.9  $\pm$ 20.2  $\mu$ m, which is similar to values reported for similar graphitic SC-ISEs.<sup>36</sup> The dried SC-ISE were then conditioned in either 1 mM NH<sub>4</sub>Cl (NH<sub>4</sub><sup>+</sup>-selective electrodes) or 1 mM KNO<sub>3</sub> (NO<sub>3</sub><sup>-</sup>-selective electrodes) for 24 h and stored dry at room temperature when not being tested. The reference electrodes used were either a commercial 3 M Ag/AgCl reference electrode (BASi, Inc.) or Ag/AgCl paint<sup>35</sup> as

Spectroscopic Characterization. A range of material characterization tests were performed to determine the laser pulse width that led to the largest increase in the electroactive nature of the LIG. Laser pulse widths of 10, 20, 30, 40, and 50 ms were tested. SEM images were taken using a FEI Quanta 250 FE-SEM (Thermo Fischer) at magnifications of 50×, 150×, and 500×. LIG samples were imaged after metal sputter-coating. X-ray photoelectron spectroscopy (XPS) measurements were performed using a Kratos Amicus/ESCA 3400 instrument. The sample was irradiated with 240 W monochromated Mg Klpha X-rays, and photoelectrons emitted at 0° from the surface normal were energy analyzed using a DuPont type analyzer. The pass energy was set at 150 eV, and a Shirley baseline was removed from all reported spectra. CasaXPS was used to process raw data files. Raman spectroscopy measurements were performed using an XploRa Plus

confocal Raman upright microscope equipped with a 532 nm excitation source (2 mW at the sample) and a Synapse EMCCD camera (Horiba Scientific/NJ, France). A 50× air objective (Olympus, LMPlanFL) with a 0.5 numerical aperture was used to collect Raman images in the epi-direction. Raman mapping was performed over an area of  $20 \times 20 \ \mu\text{m}^2$  with a step size of  $2 \ \mu\text{m}$ . The Raman spectrum collected at each pixel was recorded over a spectral range of 600-3300 cm<sup>-1</sup> with a 1200 grooves/mm grating that corresponds to an average of two measurements with a 15 s acquisition time. All data were processed using Igor Pro 6.37 scientific analysis and graphing software (Wavemetrics, Lake Oswego, OR). The spectra were fit to a Gaussian function with a linear baseline using the multifit peak function to extract peak intensity (height).

Electrochemical Characterization. Electrochemical tests were conducted using a CHI6273E electrochemical workstation (CHI Instruments) or a National Instruments potentiostat<sup>37</sup> where the LIG electrode acted as the working electrode and an external Ag/AgCl electrode (saturated in 3 M KČl) or a Ag/AgCl tape as the reference electrode, as noted. CV scans were obtained to characterize the electroactive nature of the distinct LIG electrodes with a threeelectrode setup with a platinum wire acting as the counter electrode. CV scans were performed from -0.6 to 0.8 V in 5 mM ferro/ ferricyanide solution at a scan rate of 25 mV/s. The LIG electrodes were first conditioned by running the CV scans at least five times, after which peak oxidation and reduction currents/potentials were stable and data were recorded.

Bending tests were conducted according to our previous work,<sup>38</sup> using a VEECO FPP-5000 four-point probe to conduct sample measurements. Average sheet resistance was calculated for nine replicate tests and percent change in sheet resistance reported for each material tested. Contact angle measurements were made using a custom-built goniometer, and image analysis was conducted according to our previous work.3

Nitrogen Sensing and Soil Analysis. LIG SC-ISEs were first characterized for  $\mathrm{NH_4}^+$  or  $\mathrm{NO_3}^-$  sensing in deionized (DI) water (pH 7) using calibration procedures defined by the International Union of Pure and Applied Chemistry.<sup>39</sup> Stock NH<sub>4</sub>Cl or KNO<sub>3</sub> solution was added to increase the cell concentration in 0.5 log steps over the concentration range  $10^{-7}$ – $10^{-1}$  M. Calibration tests were performed 1-3 days after conditioning in NH<sub>4</sub>Cl. To determine response time, an empirical model was fit to the time series data for each step addition using the  $\chi^2$  method; response time ( $t_{95}$ ) was calculated as the time necessary for the sensor to reach 95% of the total signal (Figure S6 in Supporting Information). In addition, a water layer was performed by exposing LIG SC-ISE to a 0.01 M solution of target ion (NH<sub>4</sub>Cl or KNO<sub>3</sub>) for 4 h, followed by a 0.01 M solution of weakly interfering ion (NaCl) for 2 h, and finally returned to the original solution for 18 h while recording potential. Limit of detection (LOD) was calculated using the three-sigma method  $(3\sigma)$ , as previously reported.<sup>33</sup>

After calibration in DI water, soil slurries were prepared using a 1:10 (w/w) ratio of soil (NAPT Reference Sample 2011-109) to DI water. After mixing and under continuous stirring conditions, the LIG SC-ISE and reference electrode were placed into the slurry. Stable sensor readings were obtained under baseline conditions (no NH<sub>4</sub>Cl/ KNO<sub>3</sub> added) and after spiking the slurry with exogenous primary ion solution  $(10^{-2}-10^{-4} \text{ M})$ . This procedure was repeated three times with new soil slurries for each replicate and the calibration curves prepared. Next, a single-point measurement was made in a new soil slurry (n = 3) by adding  $10^{-3}$  M NH<sub>4</sub>Cl or KNO<sub>3</sub> to the sample. Calibration curves were used to calculate the observed NH<sub>4</sub><sup>+</sup> or NO<sub>3</sub><sup>-</sup> concentration, and then the value was compared to the expected reading. Recovery was calculated based on the observed and predicted differences in potential following methods common to the literature. After validating calibration of LIG in soil slurries, soil column studies were conducted as a proof-of-concept application.

Soil samples for column studies were obtained from either a field supplemented with human urine (Rich Earth Institute, REI) or from a coastal mixed hardwood site (Hapludalfs), according to our previous work.43 Hardwood soils were collected from a protected area at the

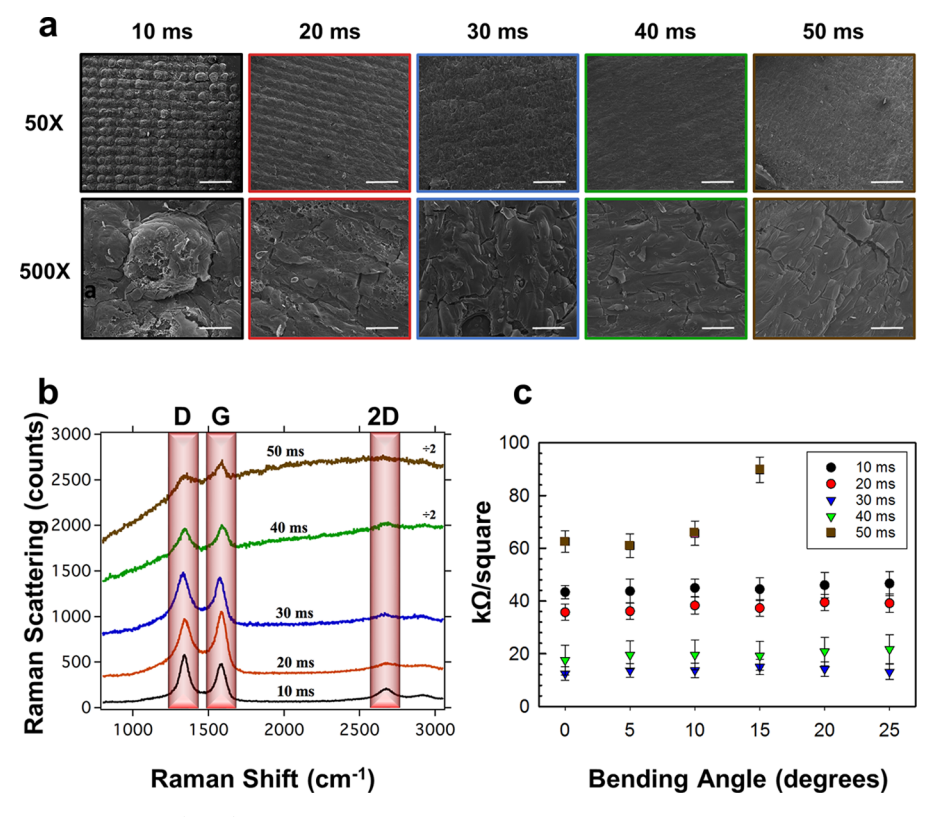


Figure 2. Scanning electron microscopy (SEM) micrographs, Raman spectra, and bending tests for LIG created with distinct laser pulse widths. Color coding refers to LIG that was created with laser pulse widths of 10 ms (black), 20 ms (orange), 30 ms (blue), 40 ms (green), and 50 ms (brown). (a) SEM images show smoother LIG surfaces with longer pulse widths, but cracking above 20 ms pulse widths. (b) Raman spectra indicate a transition from sp3 to sp2 carbon with longer pulse widths. (c) Bending tests show low deviation from unbent state at bending radii under  $30^{\circ}$  for pulse widths lower than 40 ms. Error bars represent standard deviation of the arithmetic mean (n = 3).

University of Florida Whitney Laboratory for Marine Biosciences (Marineland, FL). Five soil cores (15 cm deep) were sampled and homogenized to create a composite sample. Soil samples were packed into a 5 cm diameter, 25 cm tall clear PVC soil column (490 mL) fitted with a commercial pH probe (Fisher), NO<sub>3</sub> probe (Vernier, Beaverton, OR), and a NH<sub>4</sub><sup>+</sup> electrode (Thomas Scientific, Swedesboro, NJ). Jumper wires (Arduino) were fixed to LIG electrodes using a conductive glue (0.5:1 g-graphite powder/g-liquid tape). LIG sensors were fixed adjacent to commercial probes for all soil column studies (see Figure 5). Finally, the columns were packed with soil samples and lightly tamped. Different water samples (either DI, 1.0 mM NH<sub>4</sub>Cl, or 0.5 mM KNO<sub>3</sub>) were added to the inlet manifold at the top of the soil column as noted, and output from each electrode was recorded at a sample frequency of 300 Hz.

## ■ RESULTS AND DISCUSSION

## Sensor Development and Material Characterization.

All sensors were fabricated using adhesive Kapton polyimide sheets adhered to Epson printer paper (see Materials and Methods). The polyimide/paper substrate was treated with the pulsed UV laser at different pulse widths (10, 20, 30, 40, and 50 ms) to determine how laser energy density affected the material properties of LIG and consequently the electroactive nature of the material. First, the morphology of the LIG fabricated at distinct laser pulses was analyzed via SEM and displayed a general progressive smoothing of the graphene structure with increasing laser pulse width (Figure 2a). More specifically, LIG samples created with a laser pulse width of 10 ms were characterized by distinct rounded periodic features with high surface roughness. At laser pulse widths of 20 ms and above, these round nodule features flatten, becoming well

fused or continuous at 40 and 50 ms. Such changes in surface morphology are most likely due to the discrete, reduced heat transfer at lower pulse widths versus continuous, enhanced heat transfer at higher pulse widths. LIG created with higher pulse widths resulted in a relatively smooth, flat structure with lower surface roughness ( $R_q = 14.4 \mu m$ ), whereas LIG created with lower pulses widths resulted in stochastic formation of high-surface-area nodule structures ( $R_q = 30.9 \mu m$ ) (also see Figure S1 in the Supporting Information). These periodic features and fused surfaces each featured a high-surface-area structure, which is similar to other porous carbon materials used as transduction surfaces in SC-ISEs.<sup>25</sup> At laser pulse widths of 30 ms and above, surface cracks were observed, which consequently may have impeded electronic transport (see  $500 \times$  magnification SEM images in Figure 2a and cyclic voltammograms in Figure S5). LIG created with laser pulse widths of 20 ms exhibited a relatively well-fused surface with periodic raised patterning without noticeable cracking.

Raman spectroscopy and X-ray photoelectron spectroscopy were next used to analyze the material changes of the LIG with the distinct laser pulse treatments. The Raman spectra display prevalent D, G, and 2D bands: the D band (~1343 cm<sup>-1</sup>) corresponds to the disordered-active Raman mode, the G band (~1574 cm<sup>-1</sup>) due to C–C stretching modes is present for all graphitic materials, and the second-order Raman feature called the 2D band (~2675 cm<sup>-1</sup>), originates from second-order zone-boundary phonons.<sup>44</sup> The signal is spatially heterogeneous, as revealed by Raman maps collected over 20  $\times$  20  $\mu$ m<sup>2</sup> sample regions (see Figure S2 in the Supporting Information). The average intensity ratio  $I_D/I_G$  is a measure of the disorder

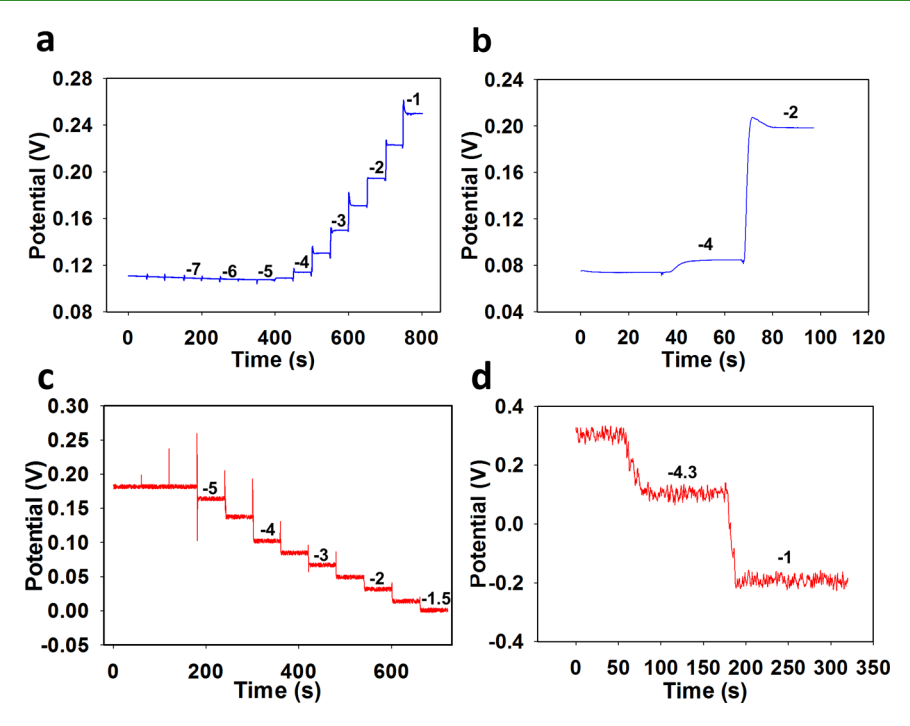


Figure 3. Open circuit potentiometry plots for NH<sub>4</sub><sup>+</sup> and NO<sub>3</sub><sup>-</sup> calibration in DI water and soil slurry solutions for the LIG SC-ISEs. NH<sub>4</sub><sup>+</sup> electrodes in (a) DI and (b) soil slurries. NO<sub>3</sub><sup>-</sup> electrodes in (c) DI and (d) soil slurries. Solution concentration of NH<sub>4</sub><sup>+</sup> or NO<sub>3</sub><sup>-</sup> (log 10 M) superimposed over real time plot in (a-d).

and defects and was calculated for each LIG sample (see Table S1 in the Supporting Information). The  $I_D/I_G$  (~1) values analyzed from the Raman spectra indicate a high degree of disorder in all of the LIG electrodes. Additionally, a clear 2D band is observed for 10 and 20 ms LIG samples. The presence of this 2D band in the Raman spectra suggests more complete graphitization of the polyimide substrate and formation of graphene layers<sup>23,33</sup> at shorter pulse widths.  $I_{\rm 2D}/I_{\rm G}$  average ratios of  $0.2 \pm 0.1$  and  $0.3 \pm 0.1$  were calculated using a Lorentzian fitting function for 10 and 20 ms samples, respectively. These values are consistent to those reported by others, whom have shown that a pulsed laser can be used to create LIG with varying degrees of graphitization of a polyimide substrate. 45,46 At longer laser pulse widths, the 2D band is not visible in the Raman spectra in combination with broadened D and G peaks with low intensity. Thus, further increase in pulse widths degrades the quality of the LIG samples, suggesting a laser-induced carbon amorphization as the sample is exposed to longer pulse widths. 47,24

XPS was performed to confirm graphene formation and measure sp<sup>2</sup> carbon atom hybridization percentages for the distinct LIG substrates (see Figure S3 in the Supporting Information). All laser pulse time displayed similar sp percentages, ranging from 76.2 to 78.3%. In particular, the 20 ms laser pulse width sample was 77% sp<sup>2</sup>. These results are on par with previous reports that have converted sp<sup>3</sup>hybridized polyimide to graphitic sp<sup>2</sup> via laser processing.<sup>24,25,34</sup>

Bending tests (concave) were conducted to investigate sensor flexibility and ensure proper sensor function with concave soil column tests (Figure 2c). Other than the sensors fabricated with a 50 ms laser pulse time, all sheet resistances changed by less than 20% for bending radii ≤30°. For the soil column studies used herein, the bending radius was  $\sim 5^{\circ}$  (see Figure S4 in the Supporting Information). On the basis of

these results, any of the LIG sensors with a laser pulse width ≤40 ms is valid for the soil column studies regarding flexibility. The lowest sheet resistance (15–20 k $\Omega$ /sq) was obtained for laser pulse width of 30-40 ms, followed by resistance of 30-40 k $\Omega$ /sq for laser pulse width of 10–20 ms, and ~60 k $\Omega$ /sq for 50 ms. For laser pulse width of 40 and 50 ms, cracking was observed at a bending radii of 30 and 15°, respectively. For laser pulse width below 40 ms, no cracking was observed below a bending radius of 45°.

To further analyze the effect of laser pulse width on electrode electroactivity, cyclic voltammetry was used to determine peak current in the presence of a negatively charged redox probe (KFeCN<sub>6</sub>). Cyclic voltammograms (see Figure S5 in the Supporting Information) displayed a quasi-reversible behavior for all LIG electrodes, with the peaks most distinct at a laser pulse width of 20 ms. 48 Similarly, highest peak current (120  $\mu$ A) and lowest peak potential separation (250 mV) were measured for LIG created with a laser pulse width of 20 ms. Peak current was lowest for LIG created with laser pulse width above 30 ms ( $\sim$ 40  $\mu$ A), and oxidative/reductive peaks were poorly defined, indicating poor electron transport.

On the basis of the analyses of morphology, surface roughness, Raman/XPS spectra, sheet resistance during bending, cracking behavior, and peak oxidative current, a laser pulse width of 20 ms was used throughout the remainder of this study for developing SC-ISE. This laser pulse width produced flexible, crack-free, high-surface-area graphene (77% sp<sup>2</sup>), with the highest peak current (120  $\mu$ A) among all conditions tested.

Sensor NH<sub>4</sub><sup>+</sup> and NO<sub>3</sub><sup>-</sup> Ion Calibration. In an effort to quantify individual sensor variability, multiple electrodes from multiple fabrication batches were fabricated using the 20 ms laser pulse width and functionalized with  $NH_4^+$  or  $NO_3^$ selective SC-ISMs (see Materials and Methods). Open circuit potentiometry plots (Figure 3a,c) were used to construct

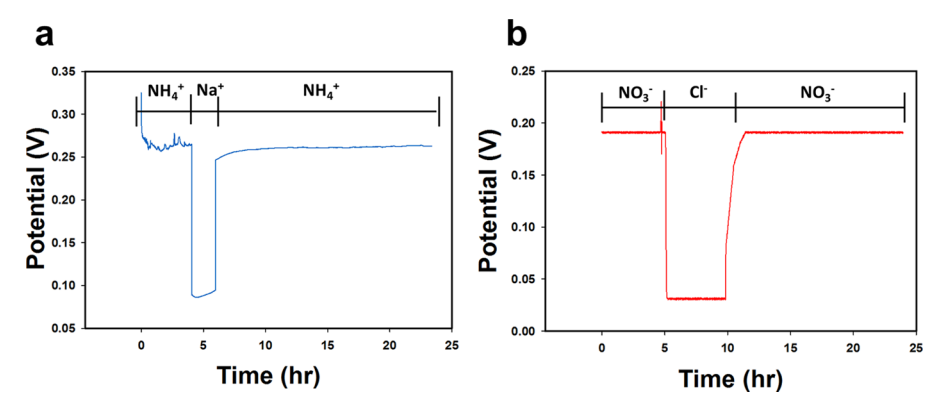


Figure 4. Representative water layer tests for NH<sub>4</sub><sup>+</sup> (a) and NO<sub>3</sub><sup>-</sup> (b) LIG SC-ISEs. Concentration for each indicated solution was 0.01 M.

calibration plots using an averaged sampling of steady-state values at a given concentration. Sensitivity and detection limit (3 $\sigma$ ) were calculated from the linear range of calibration plots for each sensor, and average response time ( $t_{95}$ ) was calculated by taking the mean of  $t_{95}$  for individual steps in the linear region. The average sensitivity for NH<sub>4</sub><sup>+</sup> electrodes in DI water was 51.7  $\pm$  7.8 mV/dec, and the average sensitivity for NO<sub>3</sub><sup>-</sup> electrodes in DI water was -54.8  $\pm$  2.5 mV/dec. The sub-Nernstian slopes are most likely the result of small molecules (H<sub>2</sub>O, CO<sub>2</sub>, and O<sub>2</sub>) that often diffuse across polymeric ISMs immobilized on solid contact electrodes and/or the result of incomplete ISM conditioning. The average limit of detection (LOD) in DI water for NH<sub>4</sub><sup>+</sup> electrodes were 28.2  $\pm$  25.0 and 20.6  $\pm$  14.8  $\mu$ M for NO<sub>3</sub><sup>-</sup> electrodes. The average  $t_{95}$  for all sensors was 5.9  $\pm$  4.1 s (see Figure S6 in the Supporting Information).

In preparation for soil column testing, SC-ISEs were further calibrated by measuring  $\mathrm{NH_4^+}$  or  $\mathrm{NO_3^-}$  in a complex soil slurry matrix spiked with  $\mathrm{NH_4Cl}$  or  $\mathrm{KNO_3}$  (Figure 3b,d). The average slope of the  $\mathrm{NH_4^+}$  LIG SC-ISE calibration equation for three different tests in said complex soil slurry was 55.2 mV  $\pm$  3.6 mV/dec, and the average slope of the  $\mathrm{NO_3^-}$  LIG SC-ISE calibration equation for five different tests was -53.4 mV  $\pm$  1.1 mV/dec. Using this equation, observed values for a single-point measurement ( $10^{-3}$  M NH<sub>4</sub>Cl or KNO<sub>3</sub>) were compared to potential values expected at this concentration. The average recovery percentages were 96% for  $\mathrm{NH_4^+}$  and 95% for  $\mathrm{NO_3^-}$  (Table S2), which demonstrate excellent sensor accuracy in a complex sensing matrix.

Experiments were performed to investigate the susceptibility of the LIG ISEs in developing an inner water layer (Figure 4). In SC-ISEs, a detrimental water layer can accumulate at the interface of the ion-selective membrane and transduction layer (LIG in this study). Previous work<sup>40</sup> has suggested that a hydrophobic surface can prevent the formation of a water layer. The measured contact angle of the LIG electrodes created with a 20 ms laser pulse width was  $80.0 \pm 0.65^{\circ}$ (indicating a surface that is nearly hydrophobic, see Figure S7), and the LIG SC-ISE did not display characteristic detrimental drift<sup>42</sup> associated with a water layer upon change of solution from primary (NH<sub>4</sub><sup>+</sup>/NO<sub>3</sub><sup>-</sup>) to weakly interfering (Na<sup>+</sup>/Cl<sup>-</sup>) ions. When a SC-ISE develops a water layer, this small volume of water acts a reservoir for ions with a composition differing from the solution being measured. When the measurement solution is changed from one containing primary ions (NH<sub>4</sub><sup>+</sup>/ NO<sub>3</sub><sup>-</sup>) to one containing interfering ions (Na<sup>+</sup>/Cl<sup>-</sup>), the water layer must come to equilibrium with the measurement solution

that does not contain the ions currently in the water layer, resulting in characteristic drift (see ref 38 for more details). Both NH<sub>4</sub><sup>+</sup> and NO<sub>3</sub><sup>-</sup> LIG SC-ISEs showed minimal drift over  $\sim$ 12 h (0.93 mV/h for NH<sub>4</sub><sup>+</sup> sensors and  $-5.3~\mu$ V/h for NO<sub>3</sub><sup>-</sup> sensors) in 0.01 M NH<sub>4</sub>Cl or 0.01 M KNO<sub>3</sub>, respectively.

 $NH_4^+$  and  $NO_3^-$  Ion Sensing in Soil Columns. To validate the LIG sensors, soil column studies were conducted with  $NH_4^+$  and  $NO_3^-$  SC-ISEs adhered to the inside of a 5 cm column and placed adjacent to corresponding  $NH_4^+$  and  $NO_3^-$  commercial ISE probes (Figure 5). Electrodes were within 1 cm of commercial electrodes and at the same column depth.

A sterilized Florida soil (hardwood) was packed into the column, and DI water was first flushed in the column (100 mL) to obtain a baseline measurement. Baseline  $\mathrm{NH_4}^+$  for LIG and commercial electrodes (0.05, and 0.03 mM, respectively) were not significantly different; similarly, baseline  $\mathrm{NO_3}^-$  for

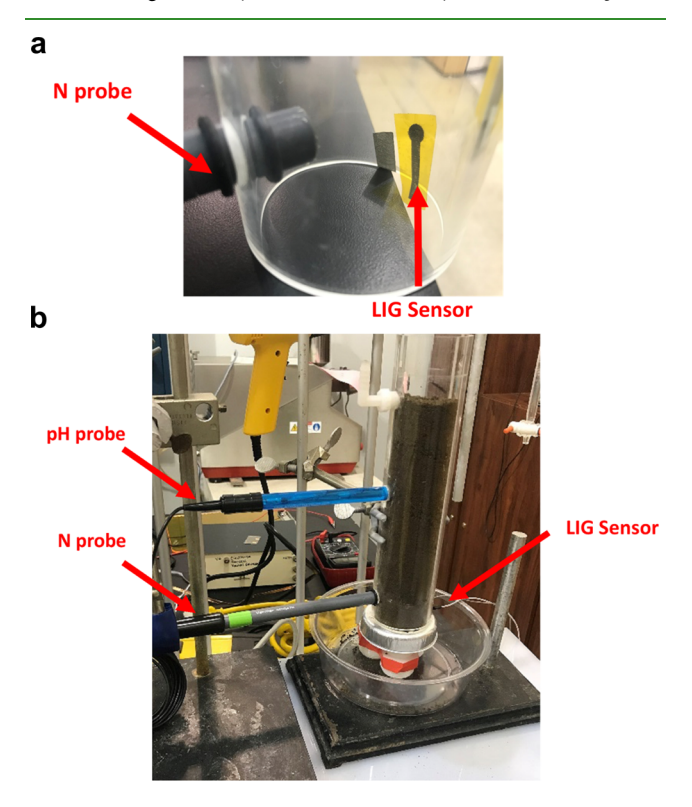


**Figure 5.** (a) Photograph of LIG-ISE and commercial nitrogen probe. Both probes were for measuring nitrate in soil column studies. (b) Soil column fitted with commercial soil sensors for measuring pH and nitrogen to validate LIG nitrogen sensors.

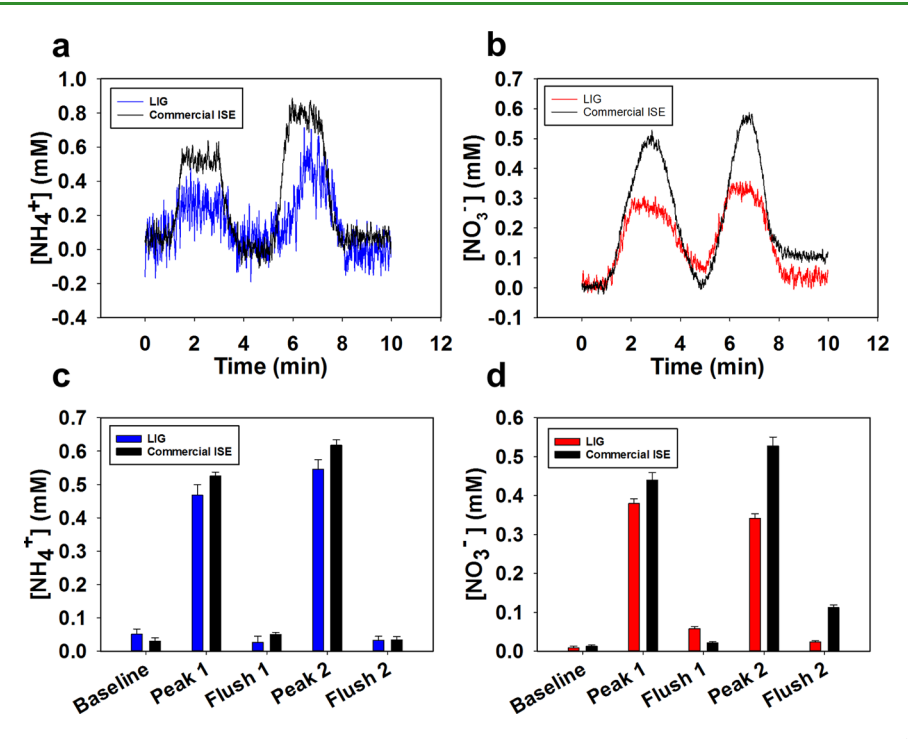


**Figure 6.** Soil column studies with LIG SC-ISEs compared to commercial ion probes. Representative real time plots of (a)  $NH_4^+$  and (b)  $NO_3^-$  ions during soil column flush experiments. Average nitrogen measured with LIG and commercial electrodes for (c)  $NH_4^+$  and (d)  $NO_3^-$  ions. Error bars represent standard deviation of the arithmetic mean (n = 3).

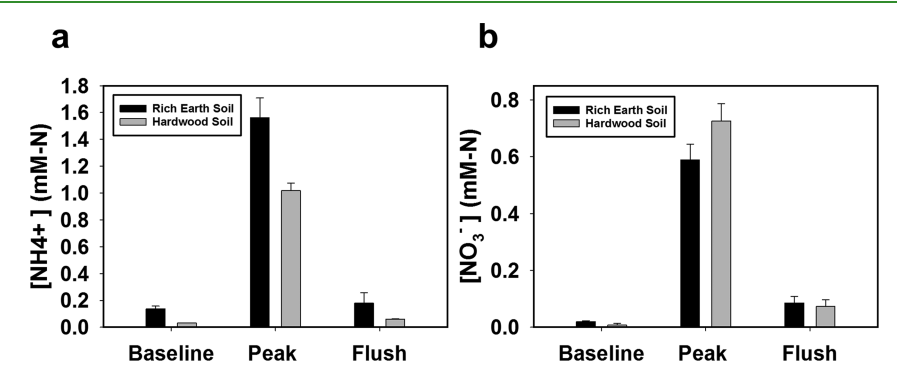


Figure 7. Soil column studies with LIG nitrogen electrodes. (a) Average  $NH_4^+$  concentration during column studies with addition of 1 mM  $NH_4$ Cl. (b) Average  $NO_3^-$  concentration during column studies with addition of 1 mM  $KNO_3$ . Error bars represent standard deviation of the arithmetic mean (n = 3).

both electrodes ( $\approx$ 0.01 mM) was not different (p < 0.0001,  $\alpha$ = 0.05). Next, 1 mM NH<sub>4</sub>Cl or 0.5 mM KNO<sub>3</sub> was added to the column in two separate pulses (Figure 6a,b). After spiking nitrogen solution, a peak signal was obtained, indicating a stable reading for each electrode (noted as "peak"), and then 100 mL of DI water was used to flush the column while recording sensor output (noted as "flush"). For all tests, the peak response and flush response occurred within 2.5 min of adding solution, and the signal was stable for at least 60 s (in some tests the electrode began to dry after reaching steady state). The average baseline, peak, and flush for two multiple cycles are shown in Figure 6c,d (n = 3 replicate tests). For all tests, the LIG SC-ISE was slightly lower than the commercial electrodes, and in most tests the commercial NO<sub>3</sub><sup>-</sup> electrodes overpredicted the NO<sub>3</sub><sup>-</sup> concentration. On the basis of an analysis of variance test, there was no significant difference (p <0.001,  $\alpha = 0.05$ ) between LIG and commercial electrodes in any test. In addition, there was no significant difference

between the response time for each electrode in the column studies.

As a final proof-of-concept, nitrogen soil column studies were repeated using LIG SC-ISEs for a nitrogen-augmented soil (noted as rich earth) and a N-deficient soil (noted as hardwood). Each column study was conducted for a load of 100 mg-N/kg-soil, which is on the high end of fertilizer loads for these types of soil.<sup>49</sup> For the NH<sub>4</sub> column studies (Figure 7a), both REI soils (138  $\pm$  20  $\mu$ M) and hardwood soils (31  $\pm$ 10 µM) had baseline levels, which were not significant, although the REI soil was significantly higher than the hardwood soil, as expected, given that the REI soil is irrigated with human urine. 50 After adding a load of 50 mg-N/kg-soil (5 g of soil), a characteristic pulse was recorded similar to the representative plots in Figure 3, and the mean of the steadystate value used to represent peak runoff nitrogen. For REI soil, the peak  $NH_4^+$  (1.6  $\pm$  0.1 mM) was significantly higher than hardwood soil (0.8  $\pm$  0.1 mM) and represented only 57% of the input N on a mass basis. This is common for NH<sub>4</sub><sup>+</sup> column

studies, as the NH<sup>4+</sup> ion readily binds to particulate matter and biological materials within the column; thus, the mobility of soil NH<sup>4+</sup> is relatively low.<sup>51</sup> After flushing the column with 100 mL of DI water, the NH<sub>4</sub><sup>+</sup> for REI (180  $\pm$  80  $\mu$ M) was higher than hardwood (60  $\pm$  40  $\mu$ M), but only slightly higher than baseline values. This effect is also expected, as the desorption rate of NH<sub>4</sub><sup>+</sup> is not homogenous as the ion is washed from the column, given the large number of functional groups, which can interact with NH<sub>4</sub><sup>+</sup>.

For the NO<sub>3</sub><sup>-</sup> column studies (Figure 7b), both REI soils  $(19 \pm 4 \,\mu\text{M})$  and hardwood soils  $(7 \pm 3 \,\mu\text{M})$  had insignificant baseline levels, with REI slightly higher than hardwood. After adding a 50 mg-N/kg-soil, the peak NO<sub>3</sub> from REI soil (589  $\pm$  55  $\mu$ M) was not as high as the hardwood soil (727  $\pm$  61 μM). These levels represent 75% and 87% recoveries of N on a mass basis for REI soil and hardwood soil, respectively, which is expected, as soil NO<sub>3</sub><sup>-</sup> is highly mobile. After a DI water flush, the NO<sub>3</sub><sup>-</sup> concentration for REI soil (85  $\pm$  23  $\mu$ M) was not significantly different than hardwood soil (73  $\pm$  25  $\mu$ M), and this remaining fraction accounts for approximately 10% of the total N load. The unaccounted fraction of NO<sub>3</sub><sup>-</sup> that remained in the column from the REI soils (approximately 10-15%) was assumed to be trapped within interstitial voids or adsorbed to biological material, although further studies are investigating this hypothesis in detail.

## CONCLUSIONS

LIG electrodes fabricated on polyimide/Epson printer paper with distinct laser pulse widths (10, 20, 30, 40, and 50 ms) were demonstrated. The simple fabrication method employed represents the first example of a SC-ISE on LIG. LIG samples created with a laser pulse width of 20 ms were determined to be the most effective electrode based on SEM, XPS, Raman spectroscopy, and CV analysis. Building on this result, LIG electrodes were functionalized with an NH<sub>4</sub><sup>+</sup> or NO<sub>3</sub><sup>-</sup> selective ionophore membrane, resulting in a SC-ISE used to measure soil nitrogen. ISEs were characterized in DI water and showed near Nernstian sensitivities of  $51.7 \pm 7.8 \text{ mV/dec} (NH_4^+)$  and  $-54.8 \pm 2.5 \text{ mV/dec (NO}_3^-)$ , detection limits of  $28.2 \pm 25.0$  $\mu$ M (NH<sub>4</sub><sup>+</sup>) and 20.6  $\pm$  14.8  $\mu$ M (NO<sub>3</sub><sup>-</sup>), and a linear sensing range of  $10^{-5}$ – $10^{-1}$  M. A water layer test indicated the absence of a detrimental water layer known to form in SC-ISEs. The LIG SC-ISE also employed within a complex sensing matrix (soil) and exhibited 96% recovery of added NH<sub>4</sub><sup>+</sup> and 95% recovery of added NO<sub>3</sub><sup>-</sup>. Soil nitrogen tests were conducted alongside commercial NO<sub>3</sub><sup>-</sup> or NH<sub>4</sub><sup>+</sup> electrodes, and the flexible LIG SC-ISEs were not significantly different, validating the use of this new low-cost electrode for measuring soil nitrogen. The overall sensing performance of the developed LIG SC-ISEs is comparable or slightly lower than comparable ISEs reported in the literature (i.e., a theoretical Nernst sensitivity of 59.2 mV/dec has been reported<sup>42</sup> and the detection limit of  $10^{-9}$  M has been reported<sup>52</sup>). However, the sensing capabilities of the LIG SC-ISEs created herein, using low-cost manufacturing (e.g., the use of a low-cost UV laser), are sufficient for low-cost fertilizer ion soil sensing and consequently present a path forward for resource-limited research laboratories and companies to create said soil sensors.

On a broader scale, these LIG-based electrodes are comparable to the recent trend of creating low-cost carbonbased electrodes via screen printing 53,54 and inkjet printing 10,55 solution-phase flakes in lieu of developing electrodes from more costly CVD graphene synthesis processes. However,

these solution-phase graphene printing techniques require metal screen masks, expensive printing equipment, development of a jettable ink, or postprint annealing processes that have complicated their fabrication. The approach described herein represents a one-step, low-cost manufacturing pathway for LIG electrodes and is the first example using LIG for use in ion sensing. Additionally, no metals, such as metallic nanoparticles, were needed to improve the electroreactive nature of the electrode, hence these LIG electrodes are amenable to scalable roll-to-roll manufacturing and suitable for use in disposable sensor technologies. Further work with these sensors could result in improved methods of in-field precision agriculture monitoring, <sup>56</sup> water quality testing, <sup>57</sup> wearable sweat biosensing and energy harvesting, <sup>58-61</sup> and point-of-care diagnostics. <sup>62-64</sup>

#### ASSOCIATED CONTENT

# S Supporting Information

The Supporting Information is available free of charge on the ACS Publications website at DOI: 10.1021/acsami.8b10991.

Schematics of electrodes used in all experiments; photograph of soil column sensor arrangement without soil; photograph of soil column with soil; optical profilometry of LIG surfaces at various laser pulse widths; Raman spectroscopy maps of the  $I_D/I_C$  ratio of a  $20 \times 20 \ \mu \text{m}^2$  area of LIG for all laser pulse widths; table of  $I_D/I_G$  ratios collected from Raman spectrograms of LIG at all laser pulse widths; XPS C 1s peak deconvolution for 20 ms LIG sample; bending tests for LIG electrodes produced at all laser pulse widths; soil slurry recovery tests for NO<sub>3</sub><sup>-</sup> and NH<sub>4</sub><sup>+</sup> LIG SC-ISEs; representative open circuit potentiometry plots (experimental and fitted model) for calculation of  $t_{95}$ ; photograph of water droplet on LIG electrode used for contact angle measurement at a laser pulse width of 20 ms (PDF)

# AUTHOR INFORMATION

#### **Corresponding Author**

\*E-mail: jcclauss@iastate.edu. Phone: 515-294-4690.

# ORCID ®

Eric S. McLamore: 0000-0002-1662-7372 Emily A. Smith: 0000-0001-7438-7808 Jonathan C. Claussen: 0000-0001-7065-1077

**Notes** 

The authors declare no competing financial interest.

# ACKNOWLEDGMENTS

J.C.C. gratefully acknowledges funding support for this work by the National Science Foundation under award number ECCS-1841649 and CBET-1706994, the National Institute of Food and Agriculture, U.S. Department of Agriculture, under award number 2016-67021-25038, as well as by the Iowa State University College of Engineering and Department of Mechanical Engineering.

### REFERENCES

(1) El-Kady, M. F.; Shao, Y.; Kaner, R. B. Graphene for Batteries, Supercapacitors and Beyond. Nat. Rev. Mater. 2016, 1, No. 16033.

(2) Kabiri Ameri, S.; Ho, R.; Jang, H.; Tao, L.; Wang, Y.; Wang, L.; Schnyer, D. M.; Akinwande, D.; Lu, N. Graphene Electronic Tattoo Sensors. ACS Nano 2017, 11, 7634-7641.

- (3) Jang, H.; Park, Y. J.; Chen, X.; Das, T.; Kim, M.-S.; Ahn, J.-H. Graphene-Based Flexible and Stretchable Electronics. Adv. Mater. 2016, 28, 4184-4202.
- (4) Geim, A. K. Graphene: Status and Prospects. Science 2009, 324, 1530-1534.
- (5) Claussen, J. C.; Kumar, A.; Jaroch, D. B.; Khawaja, M. H.; Hibbard, A. B.; Porterfield, D. M.; Fisher, T. S. Nanostructuring Platinum Nanoparticles on Multilayered Graphene Petal Nanosheets for Electrochemical Biosensing. Adv. Funct. Mater. 2012, 22, 3399-
- (6) Claussen, J. C.; Franklin, A. D.; ul Haque, A.; Porterfield, D. M.; Fisher, T. S. Electrochemical Biosensor of Nanocube-Augmented Carbon Nanotube Networks. ACS Nano 2009, 3, 37-44.
- (7) Obraztsov, A. N. Making Graphene on a Large Scale. Nat. Nanotechnol. 2009, 4, 212-213.
- (8) Kang, J.; Shin, D.; Bae, S.; Hong, B. H. Graphene Transfer: Key for Applications. Nanoscale 2012, 4, 5527-5537.
- (9) Das, S. R.; Nian, Q.; Cargill, A. A.; Hondred, J. A.; Ding, S.; Saei, M.; Cheng, G. J.; Claussen, J. C. 3d Nanostructured Inkjet Printed Graphene Via Uv-Pulsed Laser Irradiation Enables Paper-Based Electronics and Electrochemical Devices. Nanoscale 2016, 8, 15870-15879.
- (10) He, Q.; Das, S. R.; Garland, N. T.; Jing, D.; Hondred, J. A.; Cargill, A. A.; Ding, S.; Karunakaran, C.; Claussen, J. C. Enabling Inkjet Printed Graphene for Ion Selective Electrodes with Postprint Thermal Annealing. ACS Appl. Mater. Interfaces 2017, 9, 12719-12727.
- (11) Huang, X.; Leng, T.; Zhu, M.; Zhang, X.; Chen, J.; Chang, K.; Ageeli, M.; Geim, A. K.; Novoselov, K. S.; Hu, Z. Highly Flexible and Conductive Printed Graphene for Wireless Wearable Communications Applications. Sci. Rep. 2015, 5, No. 18298.
- (12) Fu, K.; Yibo, W.; Chaoyi, Y.; Yonggang, Y.; Yanan, C.; Jiaqi, D.; Steven, L.; Yanbin, W.; Jiayu, W.; Tian, L.; Zhengyang, W.; Yue, X.; Liangbing, H. Graphene Oxide-Based Electrode Inks for 3d-Printed Lithium-Ion Batteries. Adv. Mater. 2016, 28, 2587-2594.
- (13) El-Kady, M. F.; Strong, V.; Dubin, S.; Kaner, R. B. Laser Scribing of High-Performance and Flexible Graphene-Based Electrochemical Capacitors. Science 2012, 335, 1326-1330.
- (14) Lin, J.; Peng, Z.; Liu, Y.; Ruiz-Zepeda, F.; Ye, R.; Samuel, E. L.; Yacaman, M. J.; Yakobson, B. I.; Tour, J. M. Laser-Induced Porous Graphene Films from Commercial Polymers. Nat. Commun. 2014, 5, No. 5714.
- (15) Das, S. R.; Nian, Q.; Cargill, A. A.; Hondred, J. A.; Ding, S.; Saei, M.; Cheng, G. J.; Claussen, J. C. 3d Nanostructured Inkjet Printed Graphene Via Uv-Pulsed Laser Irradiation Enables Paper-Based Electronics and Electrochemical Devices. Nanoscale 2016, 8, 15870-15879.
- (16) Sepideh Khandan, D.; Rainer, B.; Andreas, B.; Heiko, S.-E.; Jiantong, L.; Torsten, K.; Mikael, Ö; Peter Haring, B.; Max, C. L. Optimizing the Optical and Electrical Properties of Graphene Ink Thin Films by Laser-Annealing. 2D Mater. 2015, 2, No. 011003.
- (17) Secor, E. B.; Gao, T. Z.; Dos Santos, M. H.; Wallace, S. G.; Putz, K. W.; Hersam, M. C. Combustion-Assisted Photonic Annealing of Printable Graphene Inks Via Exothermic Binders. ACS Appl. Mater. Interfaces 2017, 9, 29418-29423.
- (18) Secor, E. B.; Ahn, B. Y.; Gao, T. Z.; Lewis, J. A.; Hersam, M. C. Rapid and Versatile Photonic Annealing of Graphene Inks for Flexible Printed Electronics. Adv. Mater. 2015, 27, 6683-6688.
- (19) Secor, E. B.; Prabhumirashi, P. L.; Puntambekar, K.; Geier, M. L.; Hersam, M. C. Inkjet Printing of High Conductivity, Flexible Graphene Patterns. J. Phys. Chem. Lett. 2013, 4, 1347-1351.
- (20) Ye, R.; Peng, Z.; Wang, T.; Xu, Y.; Zhang, J.; Li, Y.; Nilewski, L. G.; Lin, J.; Tour, J. M. In Situ Formation of Metal Oxide Nanocrystals Embedded in Laser-Induced Graphene. ACS Nano 2015, 9, 9244-9251
- (21) Smith, M. K.; Luong, D. X.; Bougher, T. L.; Kalaitzidou, K.; Tour, J. M.; Cola, B. A. Thermal Conductivity Enhancement of Laser Induced Graphene Foam Upon P3ht Infiltration. Appl. Phys. Lett. 2016, 109, No. 253107.

- (22) Li, Y.; Luong, D. X.; Zhang, J.; Tarkunde, Y. R.; Kittrell, C.; Sargunaraj, F.; Ji, Y.; Arnusch, C. J.; Tour, J. M. Laser-Induced Graphene in Controlled Atmospheres: From Superhydrophilic to Superhydrophobic Surfaces. Adv. Mater. 2017, 29, No. 1700496.
- (23) Duy, L. X.; Peng, Z.; Li, Y.; Zhang, J.; Ji, Y.; Tour, J. M. Laser-Induced Graphene Fibers. Carbon 2018, 126, 472-479.
- (24) Lin, J.; Peng, Z.; Liu, Y.; Ruiz-Zepeda, F.; Ye, R.; Samuel, E. L. G.; Yacaman, M. J.; Yakobson, B. I.; Tour, J. M. Laser-Induced Porous Graphene Films from Commercial Polymers. Nat. Commun. 2014, 5, No. 5714.
- (25) Nayak, P.; Kurra, N.; Xia, C.; Alshareef, H. N. Highly Efficient Laser Scribed Graphene Electrodes for on-Chip Electrochemical Sensing Applications. Adv. Electron. Mater. 2016, 2, No. 1600185.
- (26) Fenzl, C.; Nayak, P.; Hirsch, T.; Wolfbeis, O. S.; Alshareef, H. N.; Baeumner, A. J. Laser-Scribed Graphene Electrodes for Aptamer-Based Biosensing. ACS Sens. 2017, 2, 616-620.
- (27) Suk, J. W.; Kitt, A.; Magnuson, C. W.; Hao, Y.; Ahmed, S.; An, J.; Swan, A. K.; Goldberg, B. B.; Ruoff, R. S. Transfer of Cvd-Grown Monolayer Graphene onto Arbitrary Substrates. ACS Nano 2011, 5, 6916-6924.
- (28) Hondred, J. A.; Breger, J. C.; Alves, N. J.; Trammell, S. A.; Walper, S. A.; Medintz, I. L.; Claussen, J. C. Printed Graphene Electrochemical Biosensors Fabricated by Inkjet Maskless Lithography for Rapid and Sensitive Detection of Organophosphates. ACS Appl. Mater. Interfaces 2018, 10, 11125-11134.
- (29) Hondred, J. A.; Stromberg, L. R.; Mosher, C. L.; Claussen, J. C. High-Resolution Graphene Films for Electrochemical Sensing Via Inkjet Maskless Lithography. ACS Nano 2017, 11, 9836-9845.
- (30) Wang, D.; Min, Y.; Yu, Y.; Peng, B. Laser Induced Self-Propagating Reduction and Exfoliation of Graphite Oxide as an Electrode Material for Supercapacitors. Electrochim. Acta 2014, 141,
- (31) Lamberti, A.; Serrapede, M.; Ferraro, G.; Fontana, M.; Perrucci, F.; Bianco, S.; Chiolerio, A.; Bocchini, S. All-Speek Flexible Supercapacitor Exploiting Laser-Induced Graphenization. 2D Mater. 2017, 4, No. 035012.
- (32) Singh, S. P.; Li, Y.; Be'er, A.; Oren, Y.; Tour, J. M.; Arnusch, C. J. Laser-Induced Graphene Layers and Electrodes Prevents Microbial Fouling and Exerts Antimicrobial Action. ACS Appl. Mater. Interfaces 2017, 9, 18238-18247.
- (33) Wu, D.; Deng, L.; Mei, X.; Teh, K. S.; Cai, W.; Tan, Q.; Zhao, Y.; Wang, L.; Zhao, L.; Luo, G.; Sun, D.; Lin, L. Direct-Write Graphene Resistors on Aromatic Polyimide for Transparent Heating Glass. Sens. Actuators, A 2017, 267, 327-333.
- (34) Tehrani, F.; Bavarian, B. Facile and Scalable Disposable Sensor Based on Laser Engraved Graphene for Electrochemical Detection of Glucose. Sci. Rep. 2016, 6, No. 27975.
- (35) Vanegas, D. C.; Patiño, L.; Mendez, C.; Oliveira, D.; Torres, A.; Gomes, C.; McLamore, E. Laser Scribed Graphene Biosensor for Detection of Biogenic Amines in Food Samples Using Locally Sourced Materials. Biosensors 2018, 8, No. 42.
- (36) Fayose, T.; Mendecki, L.; Ullah, S.; Radu, A. Single Strip Solid Contact Ion Selective Electrodes on a Pencil-Drawn Electrode Substrate. Anal. Methods 2017, 9, 1213-1220.
- (37) McLamore, E. S.; Porterfield, D. M.; Banks, M. K. Non-Invasive Self-Referencing Electrochemical Sensors for Quantifying Real-Time Biofilm Analyte Flux. Biotechnol. Bioeng. 2009, 102, 791-799.
- (38) Das, S. R.; Srinivasan, S.; Stromberg, L. R.; He, Q.; Garland, N.; Straszheim, W. E.; Ajayan, P. M.; Balasubramanian, G.; Claussen, J. C. Superhydrophobic Inkjet Printed Flexible Graphene Circuits Via Direct-Pulsed Laser Writing. Nanoscale 2017, 9, 19058-19065.
- (39) Bakker, E.; Qin, Y. Electrochemical Sensors. Anal. Chem. 2006, 78, 3965-3984.
- (40) Veder, J.-P.; De Marco, R.; Clarke, G.; Chester, R.; Nelson, A.; Prince, K.; Pretsch, E.; Bakker, E. Elimination of Undesirable Water Layers in Solid-Contact Polymeric Ion-Selective Electrodes. Anal. Chem. 2008, 80, 6731-6740.
- (41) Fibbioli, M.; Morf, W. E.; Badertscher, M.; de Rooij, N. F.; Pretsch, E. Potential Drifts of Solid-Contacted Ion-Selective Electro-

- des Due to Zero-Current Ion Fluxes through the Sensor Membrane. *Electroanalysis* **2000**, *12*, 1286–1292.
- (42) Lindner, E.; Gyurcsányi, R. E. Quality Control Criteria for Solid-Contact, Solvent Polymeric Membrane Ion-Selective Electrodes. *J. Solid State Electrochem.* **2009**, *13*, 51–68.
- (43) McLamore, E. S.; Garland, J. L.; Mackowiak, C.; Desaunay, A.; Garland, N.; Chaturvedi, P.; Taguchi, M.; Dreaden, K.; Catechis, J.; Ullman, J. L. Development and Validation of an Open Source O2-Sensitive Gel for Physiological Profiling of Soil Microbial Communities. *J. Microbiol. Methods* **2014**, *96*, 62–67.
- (44) Pimenta, M. A.; Dresselhaus, G.; Dresselhaus, M. S.; Cancado, L. G.; Jorio, A.; Saito, R. Studying Disorder in Graphite-Based Systems by Raman Spectroscopy. *Phys. Chem. Chem. Phys.* **2007**, *9*, 1276–1290.
- (45) Wang, F.; Wang, K.; Dong, X.; Mei, X.; Zhai, Z.; Zheng, B.; Lv, J.; Duan, W.; Wang, W. Formation of Hierarchical Porous Graphene Films with Defects Using a Nanosecond Laser on Polyimide Sheet. *Appl. Surf. Sci.* **2017**, *419*, 893–900.
- (46) Wu, D.; Deng, L.; Mei, X.; Teh, K. S.; Cai, W.; Tan, Q.; Zhao, Y.; Wang, L.; Zhao, L.; Luo, G.; Sun, D.; Lin, L. Direct-Write Graphene Resistors on Aromatic Polyimide for Transparent Heating Glass. Sens. Actuators, A 2017, 267, 327–333.
- (47) Loisel, L.; Châtelet, M.; Giudicelli, G.; Lebihain, M.; Yang, Y.; Cojocaru, C.-S.; Constantinescu, A.; Tay, B. K.; Lebental, B. Graphitization and Amorphization of Textured Carbon Using High-Energy Nanosecond Laser Pulses. *Carbon* **2016**, *105*, 227–232.
- (48) Bard, A. J.; Faulkner, L. R. Electrochemical Methods: Fundamentals and Applications; Wiley: NY, 1980; Vol. 2.
- (49) Salvagiotti, F.; Cassman, K. G.; Specht, J. E.; Walters, D. T.; Weiss, A.; Dobermann, A. Nitrogen Uptake, Fixation and Response to Fertilizer N in Soybeans: A Review. *Field Crops Res.* **2008**, *108*, 1–13.
- (50) Noe-Hays, A.; Nace, K.; Patel, N.; Lahr, R.; Goetsch, H.; Mullen, R.; Love, N.; Aga, D.; Bott, C.; Foxman, B.; Jimenez, J.; Luo, T.; Ramadugu, K.; Wigginton, K. Urine Diversion for Nutrient Recovery and Micropollutant Management: Results from a Regional Urine Recycling Program. *Proc. Water Environ. Fed.* **2015**, 2015, 3993–4002.
- (51) Heil, J.; Vereecken, H.; Brüggemann, N. A Review of Chemical Reactions of Nitrification Intermediates and Their Role in Nitrogen Cycling and Nitrogen Trace Gas Formation in Soil. *Eur. J. Soil Sci.* **2016**, *67*, 23–39.
- (52) Mensah, S. T.; Gonzalez, Y.; Calvo-Marzal, P.; Chumbimuni-Torres, K. Y. Nanomolar Detection Limits of Cd2+, Ag+, and K+ Using Paper-Strip Ion-Selective Electrodes. *Anal. Chem.* **2014**, *86*, 7269–7273.
- (53) Bujes-Garrido, J.; Arcos-Martínez, M. J. Development of a Wearable Electrochemical Sensor for Voltammetric Determination of Chloride Ions. *Sens. Actuators, B* **2017**, 240, 224–228.
- (54) Bandodkar, A. J.; Molinnus, D.; Mirza, O.; Guinovart, T.; Windmiller, J. R.; Valdés-Ramírez, G.; Andrade, F. J.; Schöning, M. J.; Wang, J. Epidermal Tattoo Potentiometric Sodium Sensors with Wireless Signal Transduction for Continuous Non-Invasive Sweat Monitoring. *Biosens. Bioelectron.* **2014**, *54*, 603–609.
- (55) Ruecha, N.; Chailapakul, O.; Suzuki, K.; Citterio, D. Fully Inkjet-Printed Paper-Based Potentiometric Ion-Sensing Devices. *Anal. Chem.* **2017**, *89*, 10608–10616.
- (56) Kim, H.-J.; Sudduth, K. A.; Hummel, J. W. Soil Macronutrient Sensing for Precision Agriculture. *J. Environ. Monit.* **2009**, *11*, 1810–1824
- (57) Huang, H.; Chen, T.; Liu, X.; Ma, H. Ultrasensitive and Simultaneous Detection of Heavy Metal Ions Based on Three-Dimensional Graphene-Carbon Nanotubes Hybrid Electrode Materials. *Anal. Chim. Acta* **2014**, *852*, 45–54.
- (58) Jia, W.; Gabriela, V. R.; Bandodkar, A. J.; Windmiller, J. R.; Joseph, W. Epidermal Biofuel Cells: Energy Harvesting from Human Perspiration. *Angew. Chem., Int. Ed.* **2013**, *52*, 7233–7236.
- (59) Zebda, A.; Alcaraz, J.-P.; Vadgama, P.; Shleev, S.; Minteer, S. D.; Boucher, F.; Cinquin, P.; Martin, D. K. Challenges for Successful Implantation of Biofuel Cells. *Bioelectrochemistry* **2018**, 124, 57–72.

- (60) Holade, Y.; MacVittie, K.; Conlon, T.; Guz, N.; Servat, K.; Napporn, T. W.; Kokoh, K. B.; Katz, E. Pacemaker Activated by an Abiotic Biofuel Cell Operated in Human Serum Solution. *Electroanalysis* **2014**, *26*, 2445–2457.
- (61) Jia, W.; Bandodkar, A. J.; Valdés-Ramírez, G.; Windmiller, J. R.; Yang, Z.; Ramírez, J.; Chan, G.; Wang, J. Electrochemical Tattoo Biosensors for Real-Time Noninvasive Lactate Monitoring in Human Perspiration. *Anal. Chem.* **2013**, *85*, 6553–6560.
- (62) Yang, J.; Deng, S.; Lei, J.; Ju, H.; Gunasekaran, S. Electrochemical Synthesis of Reduced Graphene Sheet—Aupd Alloy Nanoparticle Composites for Enzymatic Biosensing. *Biosens. Bioelectron.* **2011**, *29*, 159–166.
- (63) Liu, Y.; Liu, Y.; Feng, H.; Wu, Y.; Joshi, L.; Zeng, X.; Li, J. Layer-by-Layer Assembly of Chemical Reduced Graphene and Carbon Nanotubes for Sensitive Electrochemical Immunoassay. *Biosens. Bioelectron.* **2012**, *35*, 63–68.
- (64) Kostarelos, K.; Novoselov, K. S. Graphene Devices for Life. *Nat. Nanotechnol.* **2014**, *9*, 744–745.